ORIGINAL RESEARCH

Progressive and Simultaneous Right and Left Atrial Remodeling Uncovered by a Comprehensive Magnetic Resonance Assessment in Atrial Fibrillation

Clara Gunturiz-Beltrán (ID), MD; Marta Nuñez-Garcia (ID), MSc, PhD; Till F. Althoff (ID), MD, PhD; Roger Borràs, MSc; Rosa M. Figueras i Ventura, MSc, PhD; Paz Garre (ID), MSc; Gala Caixal, MD; Susanna Prat-González, MD, PhD; Rosario J. Perea, MD, PhD; Eva Maria Benito (ID), MD; Jose Maria Tolosana, MD, PhD; Elena Arbelo (ID), MD, PhD; Ivo Roca-Luque (ID), MD, PhD; Josep Brugada (ID), MD, PhD; Marta Sitges (ID), MD, PhD; Lluís Mont (ID), MD, PhD*; Eduard Guasch (ID), MD, PhD*

BACKGROUND: Left atrial structural remodeling contributes to the arrhythmogenic substrate of atrial fibrillation (AF), but the role of the right atrium (RA) remains unknown. Our aims were to comprehensively characterize right atrial structural remodeling in AF and identify right atrial parameters predicting recurrences after ablation.

METHODS AND RESULTS: A 3.0 T late gadolinium enhanced–cardiac magnetic resonance was obtained in 109 individuals (9 healthy volunteers, 100 patients with AF undergoing ablation). Right and left atrial volume, surface, and sphericity were quantified. Right atrial global and regional fibrosis burden was assessed with validated thresholds. Patients with AF were systematically followed after ablation for recurrences. Progressive right atrial dilation and an increase in sphericity were observed from healthy volunteers to patients with paroxysmal and persistent AF; fibrosis was similar among the groups. The correlation between parameters recapitulating right atrial remodeling was mild. Subsequently, remodeling in both atria was compared. The RA was larger than the left atrium (LA) in all groups. Fibrosis burden was higher in the LA than in the RA of patients with AF, whereas sphericity was higher in the LA of patients with persistent AF only. Fibrosis, volume, and surface of the RA and LA, but not sphericity, were strongly correlated. Tricuspid regurgitation predicted right atrial volume and shape, whereas diabetes was associated with right atrial fibrosis burden; sex and persistent AF also predicted right atrial volume. Fibrosis in the RA was mostly located in the inferior vena cava–RA junction. Only right atrial sphericity is significantly associated with AF recurrences after ablation (hazard ratio, 1.12 [95% CI, 1.01–1.25]).

CONCLUSIONS: AF progression associates with right atrial remodeling in parallel with the LA. Right atrial sphericity yields prognostic significance after ablation.

Key Words: atrial dilatation ■ atrial fibrillation ■ atrial remodeling ■ atrial sphericity ■ late gadolinium-enhanced magnetic resonance ■ regional fibrosis ■ right atrium

Atrial fibrillation (AF) is the most frequent sustained arrhythmia in clinical practice. Among other contributors, hypertension and structural heart disease as well as AF itself promote anatomical and functional changes in atrial properties, so-called atrial remodeling, that facilitate AF instauration and maintenance. The

CLINICAL PERSPECTIVE

What Is New?

- Atrial fibrillation (AF) causes atrial structural remodeling that contributes to the arrhythmogenic substrate.
- The left atrium plays a major role in the development and maintenance of AF.
- More complex substrate and triggers located beyond the pulmonary veins seem to be involved, and the role of the right atrium remains unknown.

What Are the Clinical Implications?

- The right atrium shows a progressive remodeling process from healthy individuals to persistent AF.
- Right atrial remodeling evolves in parallel to left atrium remodeling in AF.
- Right atrial volume and sphericity predict AF recurrences after an AF ablation procedure.
- Fibrosis in the right atrium is preferentially located in the inferior vena cava–right atrium junction.

Nonstandard Abbreviations and Acronyms

CTI	cavo-tricuspid isthmus
IIR	image intensity ratio
LGE	late gadolinium enhanced
PV	pulmonary vein
RA	right atrium

structural AF arrhythmogenic substrate is composed of atrial enlargement, deformation, and increased collagen deposit.[1]

Although characterization of left atrial remodeling and its contribution to AF development and prognosis have focused most research,[2] the role of the right atrium (RA) still remains debated. Pathophysiological,[3,4] clinical,[5,6] and ablation[7,8] data support that, at least in some cases, right atrial remodeling may be central to AF mantainance.[9] However, studies focusing on the RA have been quite often overlooked because of a lack of a standardized approach and quite often are hindered by the need for invasive procedures to characterize its arrhythmogenic substrate. Late gadolinium enhanced (LGE)–cardiac magnetic resonance (CMR) appears as an attractive tool to overcome these limitations because of its accuracy in measuring cardiac chambers.[10] Moreover, recent standardized algorithms[11] support the ability of LGE-CMR to noninvasively characterize atrial fibrosis.[1,12]

Our aims for this project were to comprehensively characterize right atrial structural remodeling occurring in patients with AF, including its progression, predictive factors, and regional distribution; to correlate these changes to left atrial remodeling; and to assess whether right atrial remodeling predicts AF recurrences after ablation procedures.

METHODS

The corresponding author had full access to all the data in the study and takes responsibility for its integrity and the data analysis. The data are available upon reasonable request.

Study Design and Sample Population

A cohort of 109 individuals were included in this study: a control group composed of 9 healthy volunteers and a study group that included 100 patients with paroxysmal or persistent AF.

The control group (healthy volunteers) involved young individuals (aged 20 to 30 years) with no known comorbidities who had a cardiac LGE-CMR performed for research purposes.[11] These CMRs served as a reference for right atrial analyses, including remodeling progression and correlation to left atrial data.

The study group included patients with AF who had been referred for a first pulmonary vein (PV) isolation procedure at our center between December 2013 and September 2018. Exclusion criteria were age <18 years, claustrophobia, severe renal failure (glomerular filtration rate <30 mL/min), gadolinium allergy, poor quality of LGE-CMR, implantable devices, pregnancy, or lactation. Data from patients undergoing ablation were obtained from a prospectively collected registry at the arrhythmia unit of our center that includes clinical, ECG, echocardiographic, and LGE-CMR data. An echocardiography was obtained from all patients before ablation and analyzed following current guidelines. Those parameters with a well-known impact on AF pathology (left atrial anteroposterior diameter, left ventricular ejection fraction, and left ventricular end-diastolic diameter) as well as parameters involved in right-side function (pulmonary pressure, tricuspid regurgitation of at least a moderate intensity) were recorded. The duration of the PR interval and the QRS were measured manually from the basal ECG of all patients.

The study protocol was reviewed and approved by our institution research ethics committee (HCB/2018/0382), and all patients signed an informed consent.

LGE-CMR Acquisition and Postprocessing

An LGE-CMR was obtained in all individuals. In patients undergoing AF ablation, it was obtained <2 weeks before the ablation procedure.

Acquisition Protocol

LGE-CMR exams were obtained with a 3.0 T CMR setup for clinical use (MAGNETOM Prisma, Siemens Medical Solutions, Erlangen, Germany), as previously reported.[1] Technical specifications of the acquisition protocol are comprehensively described in Data S1. Both the CMR setup and the imaging protocol remained unaltered for the 5 years of the study. Electrical cardioversion was performed if necessary prior to the LGE-CMR to improve image acquisition and quality. Images were acquired 20 minutes after an intravenous bolus injection of 0.2 mmol/kg gadobutrol (Gadovist, Bayer Hispania, Langreo, Spain).

Postprocessing

The right and left atria were segmented using the ADAS 3D software (Galgo Medical SL, Barcelona, Spain). The contours of both the left and right atrial walls were manually drawn in each axial plane. To minimize endocardial and epicardial segmentation artifacts, ADAS built an editable 3-dimensional shell to ensure that it crossed through the wall. Pixel signal intensity maps were calculated and projected onto the 3-dimensional shell. The following structures were cut and removed from the segmented figure: PV at the ostium level, mitral valve and appendage plane (left atrium [LA]), superior and inferior cava veins at the ostium level, tricuspid valve plane, and coronary sinus (RA). Both atria of each patient were segmented by an expert investigator and reviewed by a second expert investigator to ensure optimal image processing.

Signal intensity of both atria was normalized at the pixel level using the left atrial blood pool intensity of the same patient, thereby obtaining an image intensity ratio (IIR) value for each pixel. Each IIR value was color coded as healthy (IIR<1.20), interstitial fibrosis (1.20≤IIR≤1.32), and dense scar (IIR≥1.32) using previously standardized thresholds for the LA.[11] Of note, however, formal histological validation is missing. The complete process is summarized in Figure 1.

Analysis of Atrial Remodeling Parameters

LGE-CMR remodeling parameters were automatically calculated by ADAS 3D on the final postprocessed right and left atria. Specifically, atrial fibrosis burden (total, interstitial fibrosis, and dense scar assessed as percentage over total atrial surface), atrial surface (cm^2), volume (mL), and sphericity (unitless) were recorded. Atrial sphericity is a unitless parameter that assesses atrial shape and deformation in which larger values denote a closer similitude with a sphere.[13] A heightened sphericity index has demonstrated to independently predict AF ablation outcomes in single and multicenter studies,[13–15] outperforming other atrial size
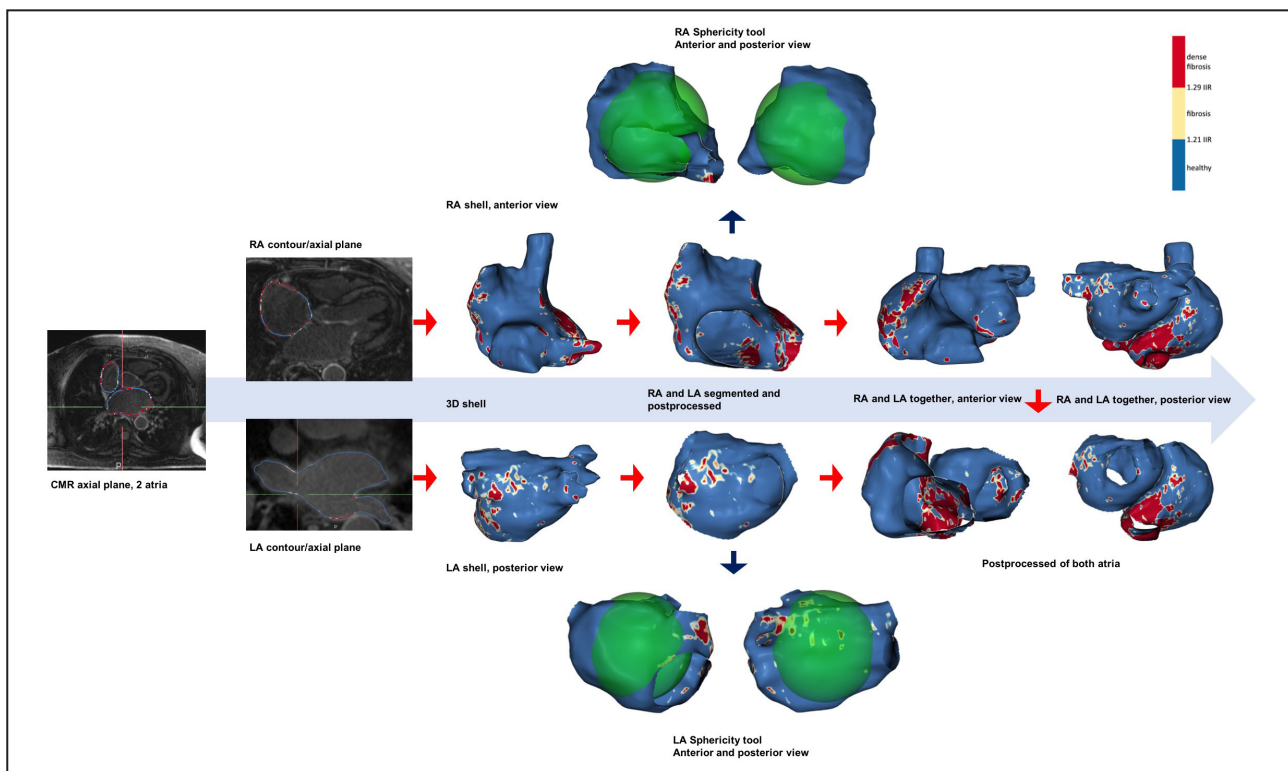

Figure 1.   Segmented and postprocessed right and left atria from CMR images.
Steps to obtain the final product for the study. 3D indicates 3-dimensional; CMR, cardiac magnetic resonance; IIR, image intensity ratio; LA, left atrium; and RA, right atrium.

parameters.[16] A comprehensive technical description of the sphericity index is provided in Data S1.

We subsequently categorized atria according to whether they had a high fibrosis burden. Because the IIR fibrosis threshold has been set at mean+2SD of the values of a healthy population,[11] healthy atria have a 2.5% fibrosis burden average. Therefore, those atria accumulating >2.5% fibrosis were considered to have a high fibrosis burden.[11,17]

Regional Fibrosis Analysis

The RA was divided into anatomically meaningful regions where the fibrosis burden was analyzed in the 3-dimensional right atrial shell.[17] First, all right atrial meshes from the 100 patients with AF were aligned and rigidly registered using as reference the right atrial shell with tricuspid valve and cava veins ostia sizes closest to the mean values in the whole data set. This reference right atrial shell was then nonrigidly registered to the remaining RA using the open-source Deformetrica software,[18] resulting in a set of right atrial meshes with point-by-point correspondence. A mean right atrial template shape was computed by averaging the registered meshes (Figure 2). We manually defined 9 segments in the averaged atrial shape surface using the open-source MeshLab software (Visual Computing Lab, Pisa, Italy). Segment boundaries were set as follows:

1. Regions 1 and 2: superior and inferior vena cava–RA junction—from the upper/lowest lateral edge of the superior/inferior vena cava at the roof/floor level to the posterior, septal, and anterior side, including the wide anatomical area of perivenous ostium with a curved line.
2. Region 3: posterior venous wall—the embryologic sinus venosus. Lateral posterior limit, the sulcus terminalis; septal limit, the interatrial sulcus at the posterior level; superior and inferior limits, the superior and inferior peri-cava vein ostia lines.
3. Region 4: posterolateral wall—internal limit, sulcus terminalis; lateral limit, from the lateral lower edge of appendage through the anatomically marked outgrowth between the posterior and vestibular lateral edges to the cavo-tricuspid isthmus (CTI) lateral line.
4. Region 5: right appendage—anatomically defined structure with anterior, lateral, and posterior borders to the roof adjacent to superior vena cava ostium.
5. Region 6: anterolateral wall—right atrial vestibule included. Lateral limit, anatomically marked outgrowth lateral border between the appendage and CTI; septal limit, the line between the roof adjacent to the superior vena cava ostium and tricuspid valve ostium at the septal level.

6. Region 7: septum—anterior limit: anterolateral wall border; posterior limit, interatrial sulcus.
7. Region 8: CTI—external line, from the lateral border of tricuspid annulus to the lateral border of the inferior vena cava ostium; internal line, from the septal border of the tricuspid annulus to the septal border of the inferior vena cava ostium.
8. Region 9: pericoronary sinus ostium (including Koch's triangle)—superior septal line, from the anterior tricuspid annulus border to the coronary sinus superior border and around it; inferior line, inner edge of the CTI.

This parcellation was automatically transferred from the averaged right atrial shape to all right atrial shells, taking advantage of the previously known point-to-point correspondence between them, thereby enabling a robust and consistent regional parcellation transfer. We carefully reviewed each computed parcellation, and manual corrections were applied to 13 cases. For each region, the percentage of fibrosis (IIR>1.20) over the total area of the region was calculated.

Ablation Procedure and Follow-Up

All patients in the ablation group underwent radiofrequency ablation at our center in accordance with standard practice using the electroanatomical navigator CARTO 3 (Biosense Webster, Diamond Bar, CA) and a multipolar, high-density mapping catheter (Lasso or Pentarray, Biosense Webster). The objective of the ablation was PV isolation, and additional left atrial lines were performed in 27% of patients with AF at the criteria of the treating electrophysiologist (posterior box in 6%, roof line in 15%, fractionated electrograms in 7%, CMR-detected fibrosis or low voltage areas in 3%, focal atrial tachycardia in 1%). If typical atrial flutter had been documented, CTI ablation was also performed.[19] No right atrial triggers were targeted or ablated.

Patients were followed at a dedicated clinic at our center at 3, 6, 12 (±1), and 24 (±4) months and annually thereafter after ablation. An ECG and a 24-hour Holter were obtained at each visit. Patients were also advised to seek for an ECG recording in case of symptoms suggestive of AF. Time to recurrence was defined as time from ablation day until first recurrence date. All patients were followed until recurrence, the 2-year visit, or May 2020, whichever occurred first. All patients were followed for at least 6 months and were censored at the last follow-up. AF lasting >30 seconds in long-term recordings or in a standard 12-lead, 10-second ECG, and occurring ≥3 months after ablation were considered to have recurred.

Statistical Analysis

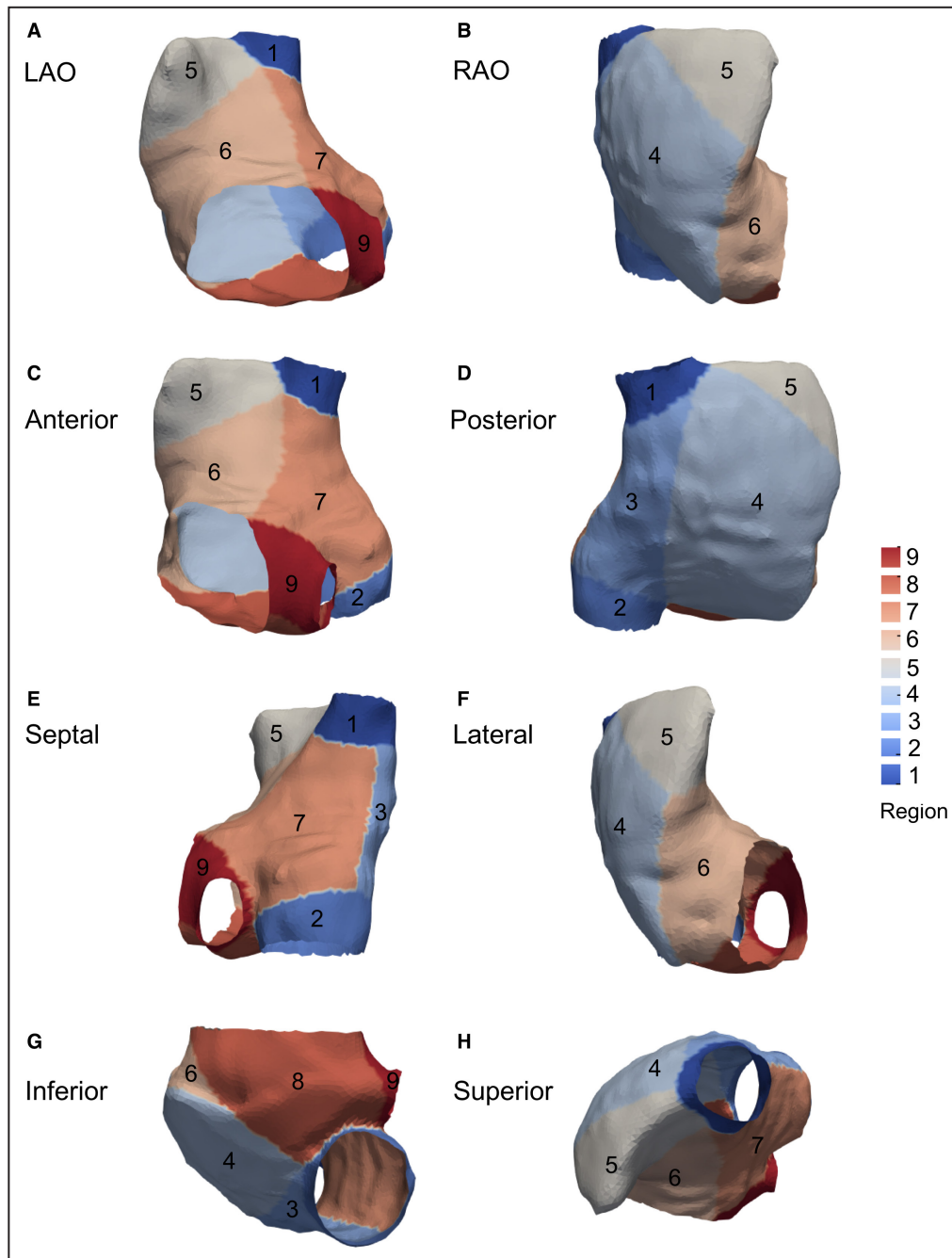Continuous variables are shown as mean±SD. Normality was assessed by visual inspection of

Figure 2. Template average of all right atria in patients with AF.
Right atrial division by 9 regional (see Methods) views: (**A**) LAO, (**B**) RAO, (**C**) anterior, (**D**) posterior, (**E**) septal, (**F**) lateral, (**G**) inferior, and (**H**) superior. AF indicates atrial fibrillation; LAO, left anterior oblique; and RAO, right anterior oblique.

the residuals in a QQ-plot. When 2 groups were compared, a *t* test or a Mann–Whitney test were used. One-way ANOVA was used for comparisons of >2 groups; post hoc pairwise comparisons were performed with false discovery rate adjustment. Correlations between parameters were analyzed by the Pearson coefficient and by modeling a linear regression model, and the interaction with group was tested by including an interaction term. Predictors of right atrial remodeling parameters were tested in univariate linear regression models, and those with a *P* value <0.1 were included in a multivariate analysis. Categorical variables were represented as absolute number and percentage,

and groups were compared with χ^2 or Fisher exact test. Recurrence predictors were tested in a Cox regression model; those with a *P* value <0.1 were included in a forward, stepwise multivariate analysis. A 5% type I error was required to reach statistical significance. All analyses were performed using R version 3.5.1 (R Project for Statistical Computing, Vienna, Austria) and SPSS version 20.0 (IBM Corp, Armonk, NY).

RESULTS

Baseline Population Characteristics

The baseline characteristics of the study population are shown in Table 1. We included 109 individuals: 9 healthy volunteers (control group) and 100 patients with AF who underwent ablation (study group). Among the latter, there were slightly more patients with paroxysmal than persistent AF (55 and 45 patients, respectively). Patients with persistent AF had a larger echocardiographic left atrial diameter and a lower, yet within the range of normality, mean ejection fraction. There were no significant differences for other clinical, ECG, or echocardiographic characteristics between both AF subgroups.

Right Atrial Characterization and Remodeling With AF Progression

We first characterized healthy RAs from young volunteers. Mean right atrial volume was 77±20mL, atrial surface was 94±16cm², fibrosis was 3.7±4.3%, and sphericity was 76.7±1.9. Progression of right atrial remodeling from healthy volunteers to paroxysmal and persistent AF was subsequently analyzed (results plotted in Figure 3). Changes in right atrial shape were evident with AF progression, including progressive dilation noted by a 2-fold increase in volume (Figure 3A), an ≈60% increase in right atrial surface (Figure 3B), and a nonsignificant (*P*=0.087) increase in sphericity denoting progressive atrial ballooning (Figure 3D). Right atrial total fibrosis remained relatively stable across groups (Figure 3C).

Correlation between right atrial size, deformation, and fibrosis were nonsignificant or of a mild intensity, similar to previous findings in the LA (Figure S1). For example, there was a low, yet significant, correlation between right atrial surface and the presence of total fibrosis in the RA (*r*=0.15, *P*=0.049), and a highly significant correlation, but of a modest intensity (*r*=0.35), between right atrial volume and sphericity. Overall, these results suggest that right atrial fibrosis, dilation and deformation develop in a different manner from healthy to diseased atria, with each parameter potentially yielding additive information.

Table 1.   **Baseline Characteristics of All Populations**

	Healthy volunteers (n=9)	Total AF (n=100)	P (healthy vs AF)	Paroxysmal AF (n=55)	Persistent AF (n=45)	P (paroxysmal vs persistent AF)
Clinical data						
Male sex	4 (44)	70 (70)	0.116	38 (69)	32 (71)	0.826
Age, y	22±0	59±11	<0.001	60±11	57±9	0.164
Weight, kg	63±11	83±14	<0.001	80±13	86±15	0.024
Height, m	168±7	170±11	0.574	169±14	172±7	0.127
Body mass index, kg/m²	22±3	29±6	0.001	29±7	29±5	0.590
Typical atrial flutter	0 (0)	11 (11)	0.294	7 (13)	4 (9)	0.542
Hypertension	0 (0)	54 (54)	0.002	29 (53)	25 (56)	0.778
Diabetes	0 (0)	9 (9)	0.347	6 (11)	3 (7)	0.461
Structural heart disease	0 (0)	20 (20)	0.138	10 (18)	10 (22)	0.615
Sleep apnea	0 (0)	11 (11)	0.294	6 (11)	5 (11)	0.974
ECG data						
PR, milliseconds	N/A	167±33		167±34	167±32	0.996
QRS, milliseconds	N/A	91±20		94±24	89±15	0.239
Echocardiographic data						
Left atrial diameter, mm	N/A	42±6		41±5	44±6	0.009
LVEF, %	N/A	58±8		59±6	56±9	0.039
PASP, mmHg	N/A	31±8		30±8	32±8	0.275
LVEDD, mm	N/A	51±6		50±5	51±6	0.478
Tricuspid regurgitation (moderate or severe)	N/A	12 (12)		4 (7)	8 (18)	0.115

Data are provided as mean±SD or number (percentage). AF indicates atrial fibrillation; LA, left atrium; LVEDD, left ventricular end diastolic diameter; LVEF, left ventricular ejection fraction; N/A, not available; and PASP, pulmonary artery systolic pressure.
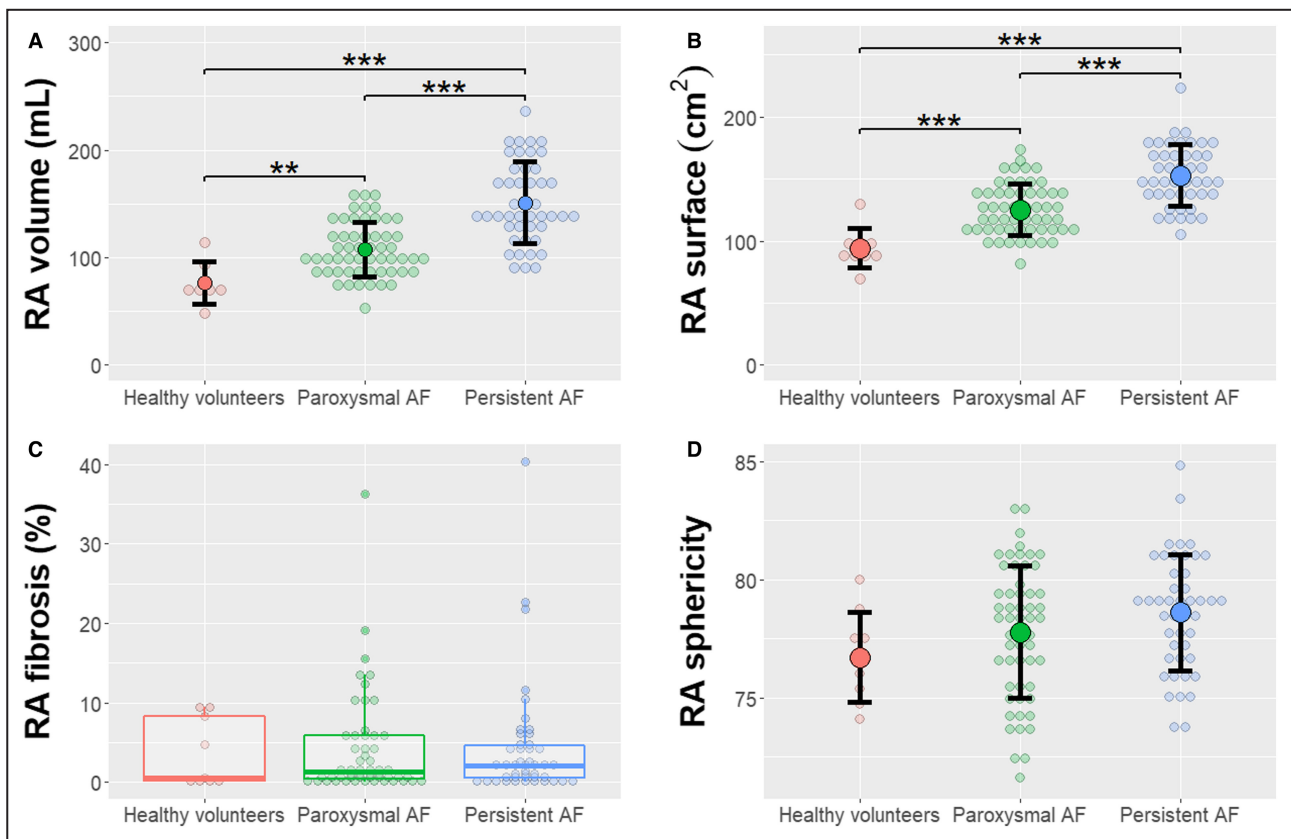
Figure 3. Progression of RA from healthy volunteers to paroxysmal and persistent AF.
Individual values and mean and SD for right atrial volume (**A**), surface (**B**), and sphericity (**D**); a boxplot is shown for right atrial fibrosis (**C**) because of data asymmetry. **$P<0.01$; ***$P<0.001$. AF indicates atrial fibrillation; and RA, right atrium.

Comparison and Correlation of Remodeling in the RA and LA

Pairwise comparisons between right and left atrial LGE-CMR remodeling parameters are shown in Table 2. In general, the RA was larger than the LA. Subgroup analyses demonstrated that the fibrosis burden was similar in the RA and LA in healthy volunteers, but in patients with paroxysmal and persistent AF, total and interstitial fibrosis were lower in the RA than in LA (both $P<0.001$). Sphericity was significantly higher in the LA than in the RA in patients with persistent AF only.

Right and left atria with a gadolinium enhancement burden >2.5% were considered to have a high fibrosis burden.[11] A total of 39 patients (39%) in the study group presented with high fibrosis in the RA, whereas it was found in the LA of 71 (71%) patients (Figure S2). Most patients who had fibrosis in the RA also did in the LA: only 2 (2%) patients had fibrosis in the RA but not in the LA. Overall, 27 (27%) patients did not have fibrosis in any atria, and 37 (37%) patients had a high fibrosis burden in both atria. Similar conclusions were reached after categorizing fibrosis into interstitial and dense scar (Figure S2).

Subsequently, we analyzed whether right atrial remodeling progressed in parallel to changes in the LA.

Results are shown in Table S1 and plotted in Figure 4. In healthy volunteers, we found a significant correlation between right and left atrial fibrosis burden ($r=0.837$, $P=0.005$), but volume and surface of both atria were uncorrelated. In contrast, total fibrosis, volume and atrial surface of the RA and LA were significantly correlated with a moderate to high intensity in both AF groups. Interestingly, right and left atrial sphericity were not correlated in either healthy volunteers or patients with AF.

Predictors of Right Atrial Remodeling

Potential clinical, ECG, and echocardiographic predictors of right atrial remodeling (ie, total fibrosis, atrial surface, and sphericity) were tested in univariate and subsequent multivariate analyses (Table S2).

Female sex was independently associated with smaller right atrial surface, whereas PR segment duration, persistent AF, and significant tricuspid regurgitation all positively associated with a larger right atrial surface. Although left ventricular ejection fraction and left atrial size predicted right atrial surface in univariate analyses, their predictive power was lost after multivariate adjustment. Tricuspid regurgitation of at least

Table 2. Comparisons of Right and Left Atrial Remodeling in the Total Population and Subgroups

	Overall		Healthy volunteers			Paroxysmal AF					
	RA	LA	RA	LA	P value	RA	LA	P value	RA	LA	P value
Volume, mL	123±39	81±33	77±20	37±9	<0.001	107±25	69±25	<0.001	151±38	103±29	<0.001
Atrial surface, cm^2	134±28	87±21	94±16	60±11	<0.001	125±21	81±17	<0.001	153±25	100±19	<0.001
Total fibrosis, %	4.1±6.7	8.9±10	3.7±4.3	5.0±6.1	0.281	4.0±6.4	8.1±8.7	<0.001	4.4±7.4	10.5±12	<0.001
Interstitial fibrosis, %	2.1±2.7	5.2±4.6	1.8±1.9	2.9±2.7	0.12	2.1±2.7	5.1±4.5	<0.001	2.2±2.7	5.9±4.9	<0.001
Dense scar, %	2.0±4.2	3.6±6.2	1.9±2.5	2.1±4.2	0.84	1.9±3.8	3±4.8	0.116	2.1±4.9	4.7±7.8	0.001
Sphericity	78±2.6	79.1±3.8	76.7±1.9	75.6±2.8	0.342	77.8±2.8	78.3±3.5	0.403	78.6±2.5	80.7±3.5	0.004

Data are provided as mean±SD. AF indicates atrial fibrillation; LA, left atrium; and RA, right atrium.

moderate intensity was the only predictor for right atrial sphericity. Finally, both bundle branch block and diabetes predicted a higher total right atrial fibrosis (percentage) in univariate analysis, but only diabetes remained as an independent predictor in multivariate analyses.

Pulmonary pressure was not included in right atrial remodeling prediction analysis because it could only be analyzed in patients with tricuspid regurgitation. Among these patients (n=49), those with pulmonary hypertension (systolic pulmonary pressure >35 mm Hg) tended to have larger RAs (131.4±40.3 mL versus 152.9±37.5 mL for patients without and with pulmonary hypertension, respectively; P=0.07), but not a higher fibrosis burden (5.8±9.3% versus 3.7±6.3%, respectively; P=0.37).

Right Atrial Remodeling and Postablation Recurrences

During a median follow-up time of 23.6 months (interquartile range, 11.1–27.2 months), 50 patients (50%) had an AF recurrence beyond the 3-month blanking period. A Cox regression analysis was performed to ascertain whether right atrial remodeling parameters predicted recurrent AF ablation (Table 3). Both right atrial volume (hazard ratio [HR], 1.07 [95% CI, 1.00–1.14]) and right atrial sphericity (HR, 1.12 [95% CI, 1.01–1.25]) were predictors of AF recurrence in univariate analysis and were included in multivariate analysis, but the latter was the unique independent predictor factor (right atrial sphericity: HR, 1.12 [95% CI, 1.01–1.25]). Incorporating LA-related parameters into multivariate analysis did not modify conclusions. Adding extra PV ablation lines did not decrease postablation recurrences (HR, 0.68 [95% CI, 0.37–1.23]).

Regional Fibrosis Analysis

Atrial fibrosis was not uniformly distributed along the right atrial wall (Figure 5). Regional fibrosis analyses demonstrated highly significant differences between regions (omnibus P<0.001) (Figure 6). Pairwise comparisons between all regions are shown in Figure S3.

The largest fibrosis burden was located in the inferior vena cava–RA junction (region 2), with a mean fibrosis of 22% (95% CI, 19–24). This was almost 6-fold higher than the overall right atrial fibrosis and significantly higher than all other regions. Fibrosis was also relevant in regions 7 (septum), 3 (posterior venous wall), and 9 (pericoronary sinus ostium), although they were not significantly different than other regions (except when compared with region 2). The study workflow and results were summarized in Figure 7.

DISCUSSION

In this article, we report the results of a comprehensive analysis of right atrial remodeling in a large cohort of patients with AF and healthy volunteers. The main findings are that (1) the RA enters a progressive remodeling process from healthy individuals to persistent AF characterized by enlargement and deformation; (2) except for sphericity, atrial remodeling evolves simultaneously in the RA and LA; (3) right atrial volume and sphericity predict AF recurrences after an AF ablation procedure, but only sphericity remains as an independent predictor; and (4) right atrial fibrosis is usually localized in the inferior vena cava–RA junction.

AF Associates With Progressive Right Atrial Remodeling

Clinical insights suggest a role for the RA in AF development. Chronic obstructive pulmonary disease, pulmonary hypertension, and congenital heart disease impose a hemodynamic overload in right-sided chambers.[5,20] In studies conducted in patients undergoing ablation, extrapulmonary ectopic foci have been occasionally found in the RA,[7,8] and the RA might drive AF in up to 20% of patients with persistent AF.[21] Experimental studies further support that the RA may sustain AF in some cases. Allessie and collaborators found that sustained AF was more readily inducible in those animals with right atrial dilation than in those with left atrial dilation.[3] In a pulmonary hypertension mouse model, right atrial reentrant activity sustained
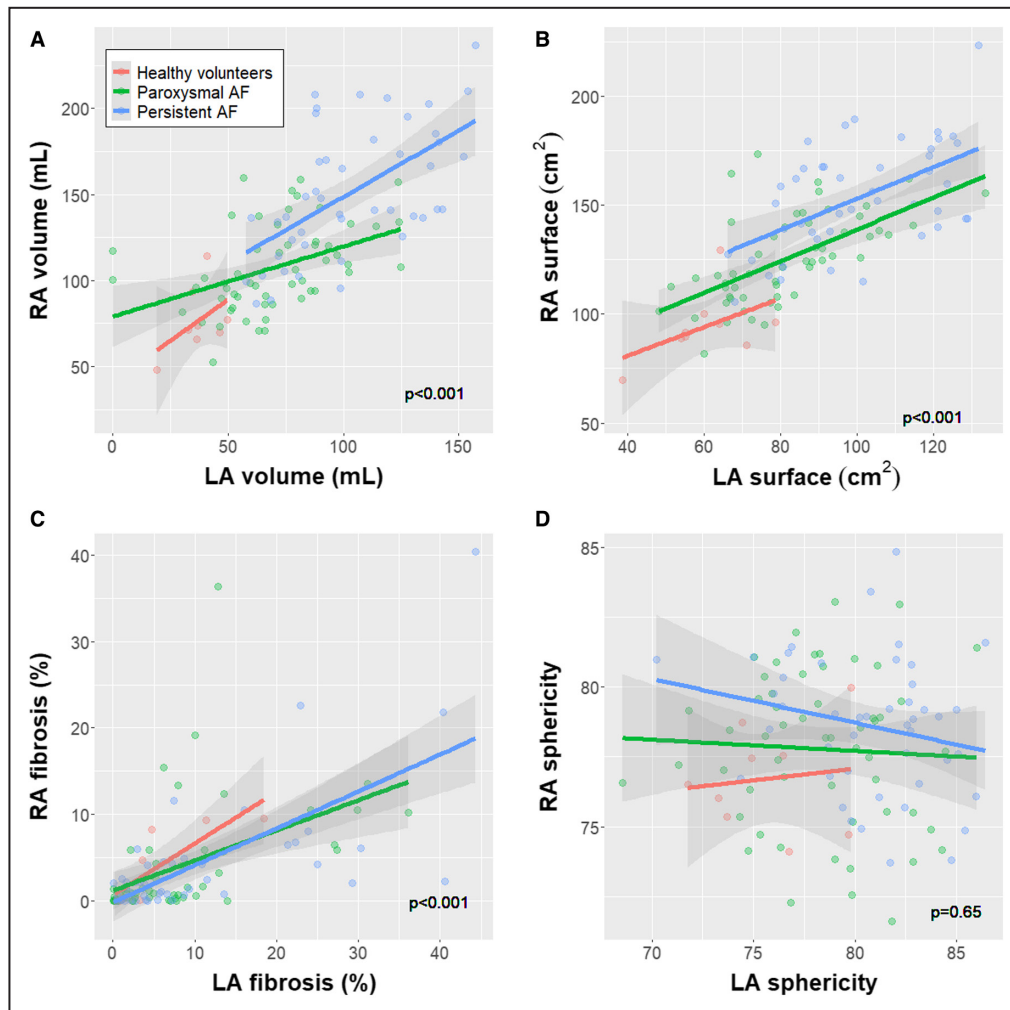
Figure 4. Correlation between remodeling parameters in the RA and LA.
The correlation between right and left atrial volume (**A**), surface (**B**), fibrosis (**C**), and sphericity (**D**) is plotted. The *P* value reports the significance of the correlation in a linear regression model. The interaction term including the group was nonsignificant in all cases. AF indicates atrial fibrillation; LA, left atrium; and RA, right atrium.

AF.[4] However, right atrial remodeling has been scarcely studied in patients with AF. Echocardiographic[22] and electrophysiologic[23] studies suggested right atrial dilation, conduction velocity slowing, and electrogram fragmentation in patients with AF compared with those in sinus rhythm. Nevertheless, only right atrial volume has been studied.

In this article, we use LGE-CMR to show that AF associates with progressive right atrial remodeling from healthy volunteers to persistent AF. Interestingly, each of the right atrial remodeling markers seemed to develop independently of the other atrial remodeling parameters. Right atrial dilation occurred early in AF development, increased sphericity evolves only in later stages what substantiates its role as the strongest and only independent factor of AF recurrence after ablation in our study; while no significant changes could be identified for atrial fibrosis. The lack of a robust and strong correlation between them supports that

information yielded by each marker is additive to the remaining ones.

Myocardial Fibrosis in the RA Is Heterogeneously Distributed and Is Not Increased in Patients With AF

Histological analysis in patients undergoing surgery or in necropsy specimens show that fibrosis burden is higher in the RA of patients with AF than those in sinus rhythm.[24] Nevertheless, conflicting results have also been published.[25,26] Our results support the latter and suggest that right atrial fibrosis remains relatively stable during the course of AF development. Differences in the methodology may explain these apparently contradictory conclusions. The heterogeneous distribution of fibrosis in the RA limits the ability of histological analysis to characterize the whole-atrial fibrosis burden through the analysis of small samples; conversely, LGE-CMR

Table 3. Right Atrial Remodeling Parameters Predictive of Recurrences After AF Ablation (Out of Blanking Period)

	Univariate			Multivariate		
	HR	95% CI	*P* value	HR	95% CI	*P* value
Volume, per 10 mL	1.067	1.000–1.138	0.052			
Area, per 10 cm²	1.081	0.983–1.189	0.106			
Total fibrosis, %	1.014	0.979–1.051	0.44			
Interstitial fibrosis, %	1.035	0.938–1.143	0.49			
Dense scar, %	1.021	0.969–1.077	0.44			
Sphericity	1.121	1.006–1.248	0.038	1.121	1.006–1.248	0.038

AF indicates atrial fibrillation; and HR, hazard ratio.

enabled us to estimate whole-atrial fibrosis. Moreover, we only included patients who planned to undergo AF ablation, and those with permanent AF, who are likely to have more diseased atria, were excluded. In contrast, surgical specimens are commonly obtained in patients with permanent AF. Finally, we cannot rule out some minor degree of right atrial fibrosis in those patients at more advanced AF stages that could not be captured because of the insufficient statistical power of our study. Of note, the estimated difference between healthy volunteers and patients with persistent AF (0.7% [95% CI, −4.14% to 5.54%]) cannot rule out a difference in right atrial fibrosis as large as 5.5%. In any case, our results show that right atrial fibrosis is substantially lower than that of the LA. Consistent with this finding, an experimental study in an animal model found that, although right and left atrial fibrosis burden were similar in healthy animals, left atrial fibrosis was remarkably higher than right atrial fibrosis in animals with AF.[27]

Current evidence suggests that atrial fibrosis accumulates in specific areas. In the LA, work in LGE-CMR found that fibrosis clustered in the posterior wall and floor around the left inferior PV.[17] Interestingly, the close anatomical relationship between these areas and the descending aorta has been recently claimed to potentially contribute to fibrosis accumulation by means of continuous and repetitive microtrauma.[28] Right atrial fibrosis localization had not been systematically assessed. By mean of rough visual inspection, Akoum and coworkers suggested that the most affected areas were the septum, superior and inferior peri-cava veins and posterior venous wall.[29] By taking advantage of a systematic workflow and robust algorithms, we found that fibrosis generally located septally, involving the RA–inferior vena cava junction, septum, posterior venous wall, and pericoronary sinus ostium. Although our work was not designed to ascertain their potential causes, these areas are close to the junction with the LA, in contact with the ascending aorta (Figure S4), may be involved in lipomatous hypertrophy in some cases, and share a common embryological origin (ie, the initial invagination of the right atrial wall that forms the embryological septum secundum).

Right Atrial Remodeling Is Associated With Hemodynamic Overload and Systemic Conditions

We assessed which factors might contribute to right atrial changes occurring with AF. Hemodynamic overload was particularly associated with geometrical remodeling. Tricuspid regurgitation of at least a moderate
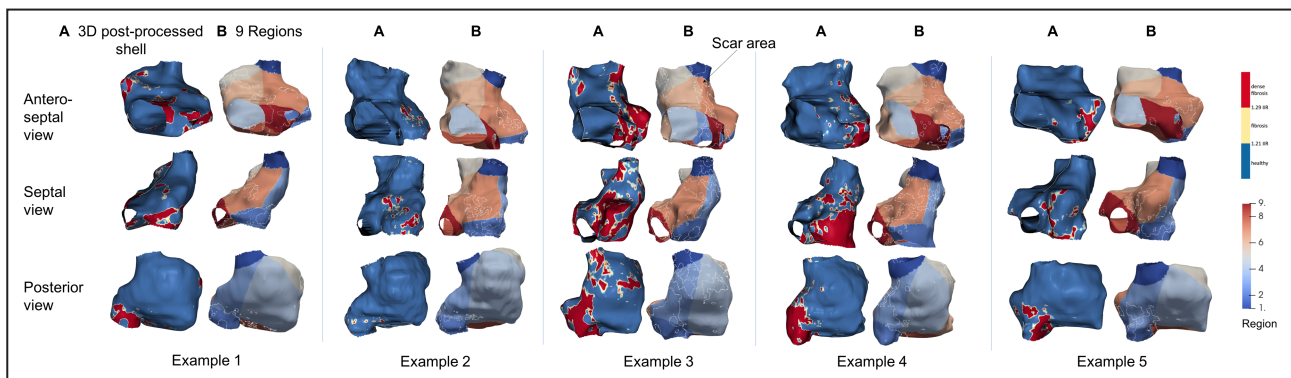

Figure 5. Examples of fibrosis localization in the right atrium.
A total of 5 examples are shown, and 3 views are provided for each. In each example, fibrosis is shown in the 3D postprocessed color-coded shell constructed by ADAS software (fibrosis in red) (**A**) and after being transferred to the 9-region template (**B**). 3D indicates 3-dimensional; and IIR, image intensity ratio.
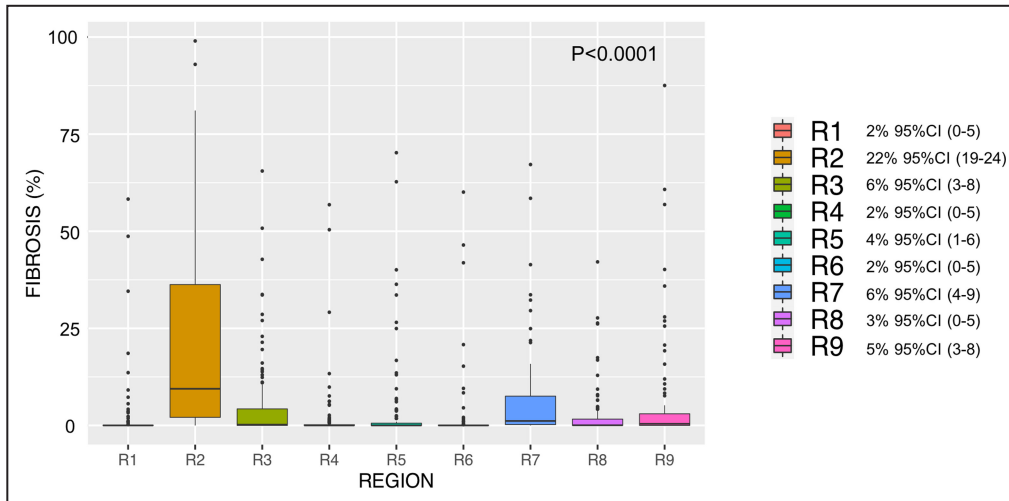
Figure 6. Regional distribution of right atrial fibrosis.
Boxplot diagram for each region representing fibrosis (percentage) (median and 95% CI). R indicates region.

degree was associated with larger and deformed RA, whereas pulmonary hypertension seemed to associate with a right atrial enlargement of ≈20 mL (*P*=0.07).

Surprisingly, despite hemodynamic overload, diabetes was the strongest predictor of right atrial fibrosis. The dependence of right atrial fibrosis on systemic
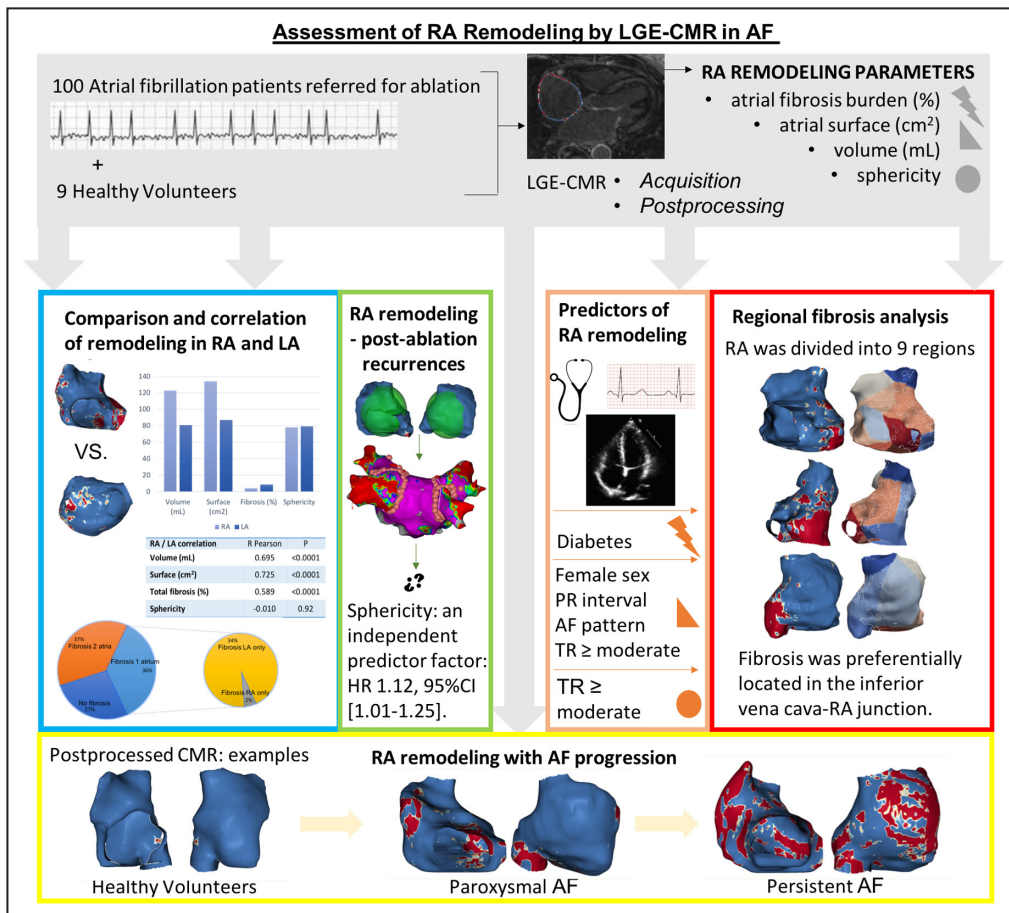

Figure 7. Assessment of right atrial remodeling by LGE-CMR in AF: summary study workflow and results.
AF indicates atrial fibrillation; CMR, cardiac magnetic resonance; HR, hazard ratio; LA, left atrium; LGE, late gadolinium enhanced; RA, right atrium; and TR, tricuspid regurgitation.

conditions is supported by recent work in a pulmonary hypertension animal model in which right atrial fibrosis fully recovered after targeting inflammation, whereas right atrial dilation remained unaltered.[30]

Limitations

Some limitations of our work should be acknowledged. Image acquisition and postprocessing could be a common source of inaccuracies. Although we have previously proved good intra- and interobserver reproducibility even in the hands of nonexperienced operators,[31] small errors in technical parameters may still be relevant. Specifically, the reproducibility of the sphericity index, although excellent in the LA,[13] has never been tested in the RA. Notably, most parameters are automatically calculated once images have been segmented, thereby blunting any observation bias. An intrinsic limitation of the technique is that LGE represents fibrosis but also may flag inflammation or portions of venous embryologic origin. Moreover, the inferior vena cava commonly extends into the posterior and inferior aspect of the RA[32] and could artifact fibrosis burden measurements, particularly in regions 2 and 3. Validating LGE-CMR findings with intracavitary voltage may help to elucidate these limitations. Finally, we could only test for associations, and causality cannot be claimed from our study.

CONCLUSIONS

The analysis of right atrial remodeling using LGE-CMR is feasible and shows dilation and spheronization with progression from healthy individuals to persistent AF. Right atrial fibrosis localizes in the RA–inferior vena cava junction and remains almost stable at all stages. There is a high right-to-left correlation for atrial volume and fibrosis, but not for sphericity. Sphericity was the strongest predictor for AF recurrence after ablation. These results may be useful to predict AF incidence and recurrence after ablation and to plan individualized strategies for AF therapy, but these need to be tested in dedicated studies.

ARTICLE INFORMATION

Affiliations

Arrhythmia Section, Institut Clínic Cardiovascular, Hospital Clínic, Universitat de Barcelona, Barcelona, Catalonia, Spain (C.G., T.F.A., R.B., P.G., G.C., S.P., R.J.P., E.M.B., J.M.T., E.A., I.R., J.B., M.S., L.M., E.G.); Institut d'Investigacions Biomédiques August Pi i Sunyer, Barcelona, Catalonia, Spain (C.G., R.B., P.G., G.C., S.P., R.J.P., E.M.B., J.M.T., E.A., I.R., J.B., M.S., L.M., E.G.); Centro de Investigación Biomédica en Red de Enfermedades Cardiovasculares, Instituto de Salud Carlos III, Madrid, Spain (C.G., S.P., R.J.P., J.M.T., E.A., I.R., J.B., M.S., L.M., E.G.); Electrophysiology and Heart Modeling Institute (IHU LIRYC), Pessac, France (M.N.); Université de Bordeaux, Bordeaux, France (M.N.); Department of Cardiology and Angiology, Charité, University Medicine Berlin, Charité Campus Mitte, Berlin, Germany (T.F.A.); DZHK (German Centre for Cardiovascular Research), Partner Site Berlin, Berlin, Germany (T.F.A.); Centro de Investigación Biomédica en Red de Salud Mental, Instituto de Salud Carlos III, Madrid, Spain (R.B.); and ADAS 3D Medical SL, Barcelona, Catalonia, Spain (R.M.F.i.).

Sources of Funding

Disclosures

Supplemental Material

Data S1
Tables S1–S2
Figures S1–S4

REFERENCES

1. den Uijl DW, Cabanelas N, Benito EM, Figueras R, Alarcón F, Borràs R, Prat S, Guasch E, Perea R, Sitges M, et al. Impact of left atrial volume, sphericity, and fibrosis on the outcome of catheter ablation for atrial fibrillation. *J Cardiovasc Electrophysiol.* 2018;29:740–746. doi: 10.1111/jce.13482

2. McGann C, Akoum N, Patel A, Kholmovski E, Revelo P, Damal K, Wilson B, Cates J, Harrison A, Ranjan R, et al. Atrial fibrillation ablation outcome is predicted by left atrial remodeling on MRI. *Circ Arrhythmia Electrophysiol.* 2014. 7, 23, 30, doi: 10.1161/CIRCEP.113.000689. Available from: http://www.ncbi.nlm.nih.gov/pubmed/24363354

3. Zarse M, Deharo JC, Mast F, Allessie MA. Importance of right and left atrial dilation and linear ablation for perpetuation of sustained atrial fibrillation. *J Cardiovasc Electrophysiol.* 2002;13:164–171. doi: 10.1046/j.1540-8167.2002.00164.x

4. Hiram R, Naud P, Xiong F, Al-U'datt D, Algalarrondo V, Sirois MG, Tanguay J-F, Tardif J, Nattel S. Right atrial mechanisms of atrial fibrillation in a rat model of right heart disease. *J Am Coll Cardiol.* 2019;74:1332–1347. doi: 10.1016/j.jacc.2019.06.066

5. Grymonprez M, Vakaet V, Kavousi M, Stricker BH, Ikram MA, Heeringa J, Franco OH, Brusselle GG, Lahousse L. Chronic obstructive pulmonary disease and the development of atrial fibrillation. *Int J Cardiol.* 2019;276:118–124. doi: 10.1016/j.ijcard.2018.09.056

6. Guasch E, Mont L. Diagnosis, pathophysiology, and management of exercise-induced arrhythmias. *Nat Rev Cardiol.* 2017;14:88–101. doi: 10.1038/nrcardio.2016.173

7. Santangeli P, Marchlinski FE. Techniques for the provocation, localization, and ablation of non-pulmonary vein triggers for atrial fibrillation. *Heart Rhythm.* 2017;14:1087–1096. doi: 10.1016/j.hrthm.2017.02.030. Available from: http://www.ncbi.nlm.nih.gov/pubmed/28259694

8. Lin W-S, Tai C-T, Hsieh M-H, Tsai C-F, Lin Y-K, Tsao H-M, Huang J-L, Yu W-C, Yang S-P, Ding Y-A, et al. Catheter ablation of paroxysmal atrial fibrillation initiated by non-pulmonary vein ectopy. *Circulation.* 2003;107:3176–3183. doi: 10.1161/01.CIR.0000074206.52056.2D

9. Hasebe H, Yoshida K, Iida M, Hatano N, Muramatsu T, Nogami A, Aonuma K. Differences in the structural characteristics and distribution of epicardial adipose tissue between left and right atrial fibrillation. *Europace.* 2018;20:435–442. doi: 10.1093/europace/eux051

10. Maceira AM, Cosin-Sales J, Prasad SK, Pennell DJ. Characterization of left and right atrial function in healthy volunteers by cardiovascular magnetic resonance. *J Cardiovasc Magn Reson.* 2016;18:1–16.

11. Benito EM, Carlosena-Remirez A, Guasch E, Prat-González S, Perea RJ, Figueras R, Borràs R, Andreu D, Arbelo E, Tolosana JM, et al. Left atrial fibrosis quantification by late gadolinium-enhanced magnetic resonance: a new method to standardize the thresholds for reproducibility. *Europace.* 2017;19:1272–1279. doi: 10.1093/europace/euw219

12. Linhart M, Alarcon F, Borràs R, Benito EM, Chipa F, Cozzari J, Caixal G, Enomoto N, Carlosena A, Guasch E, et al. Delayed gadolinium enhancement magnetic resonance imaging detected anatomic gap length in wide circumferential pulmonary vein ablation lesions is associated with recurrence of atrial fibrillation. *Circ Arrhythm Electrophysiol.* 2018;11:e006659. Available from: http://www.ncbi.nlm.nih.gov/pubmed/30562102

13. Bisbal F, Guiu E, Calvo N, Marin D, Berruezo A, Arbelo E, Ortiz-Pérez J, de Caralt TM, Tolosana JM, Borràs R, et al. Left atrial sphericity: a new method to assess atrial remodeling. Impact on the outcome of atrial fibrillation ablation. *J Cardiovasc Electrophysiol.* 2013;24:752–9. Available from: http://www.ncbi.nlm.nih.gov/pubmed/23489827

14. Bisbal F, Alarcón F, Ferrero-de-Loma-Osorio A, González-Ferrer JJ, Alonso C, Pachón M, Tizón H, Cabanas-Grandío P, Sanchez M, Benito E, et al. Left atrial geometry and outcome of atrial fibrillation ablation: results from the multicentre LAGO-AF study. *Eur Heart J Cardiovasc Imaging.* 2018;19:1002–1009. Available from: http://www.ncbi.nlm.nih.gov/pubmed/29659784

15. Nakamori S, Ngo LH, Tugal D, Manning WJ, Nezafat R. Incremental value of left atrial geometric remodeling in predicting late atrial fibrillation recurrence after pulmonary vein isolation: a cardiovascular magnetic resonance study. *J Am Heart Assoc.* 2018;7:e009793. Available from: http://www.ncbi.nlm.nih.gov/pubmed/30371333

16. Varela M, Bisbal F, Zacur E, Berruezo A, Aslanidi O V, Mont L, Lamata P. Novel computational analysis of left atrial anatomy improves prediction of atrial fibrillation recurrence after ablation. *Front Physiol.* 2017;8:68. Available from: http://www.ncbi.nlm.nih.gov/pubmed/28261103

17. Benito EM, Cabanelas N, Nuñez-Garcia M, Alarcón F, Figueras I Ventura RM, Soto-Iglesias D, Guasch E, Prat-Gonzalez S, Perea RJ, Borràs R, et al. Preferential regional distribution of atrial fibrosis in posterior wall around left inferior pulmonary vein as identified by late gadolinium enhancement cardiac magnetic resonance in patients with atrial fibrillation. *Europace.* 2018;20:1959–1965. Available from: http://www.ncbi.nlm.nih.gov/pubmed/29860416

18. Bône A, Louis M, Martin B, Durrleman S. Deformetrica 4: an open-source software for statistical shape analysis. In: Reuter M, Wachinger C, Lombaert H, Paniagua B, Lüthi M, Egger B, eds. *Lecture Notes in Computer Science (Including Subseries Lecture Notes in Artificial Intelligence and Lecture Notes in Bioinformatics).* Springer, Cham; 2018:3–13. Available from: https://link.springer.com/chapter/10.1007/978-3-030-04747-4_1

19. Calkins H, Hindricks G, Cappato R, Kim Y-H, Saad EB, Aguinaga L, Akar JG, Badhwar V, Brugada J, Camm J, et al. 2017 HRS/EHRA/ECAS/APHRS/SOLAECE expert consensus statement on catheter and surgical ablation of atrial fibrillation: executive summary. *Europace.* 2018;20:157–208. doi: 10.1093/europace/eux275. Available from: http://www.ncbi.nlm.nih.gov/pubmed/29016841

20. Drakopoulou M, Nashat H, Kempny A, Alonso-Gonzalez R, Swan L, Wort SJ, Price LC, McCabe C, Wong T, Gatzoulis MA, et al. Arrhythmias in adult patients with congenital heart disease and pulmonary arterial hypertension. *Heart.* 2018;104:1963–1969.

21. Hocini M, Nault I, Wright M, Veenhuyzen G, Narayan SM, Jaïs P, Lim KT, Knecht S, Matsuo S, Forclaz A, et al. Disparate evolution of right and left atrial rate during ablation of long-lasting persistent atrial fibrillation. *J Am Coll Cardiol.* 2010;55:1007–1016. doi: 10.1016/j.jacc.2009.09.060

22. Zatuchni J. Atrial enlargement as a consequence of atrial fibrillation. *Circulation* 1991;83:1458. Available from: https://www.ahajournals.org/doi/10.1161/circ.83.4.1826477

23. Stiles MK, John B, Wong CX, Kuklik P, Brooks AG, Lau DH, Dimitri H, Roberts-Thomson KC, Wilson L, De Sciscio P, et al. Paroxysmal lone atrial fibrillation is associated with an abnormal atrial substrate. Characterizing the "second factor". *J Am Coll Cardiol.* 2009;53:1182–1191. Available from: http://www.ncbi.nlm.nih.gov/pubmed/19341858

24. Platonov PG, Mitrofanova LB, Orshanskaya V, Ho SY. Structural abnormalities in atrial walls are associated with presence and persistency of atrial fibrillation but not with age. *J Am Coll Cardiol.* 2011;58:2225–2232. doi: 10.1016/j.jacc.2011.05.061

25. Nakai T, Chandy J, Nakai K, Bellows WH, Flachsbart K, Lee RJ, Leung JM. Histologic assessment of right atrial appendage myocardium in patients with atrial fibrillation after coronary artery bypass graft surgery. *Cardiology.* 2007;108:90–96. doi: 10.1159/000095936

26. Smorodinova N, Lantová L, Bláha M, Melenovský V, Hanzelka J, Pirk J, Kautzner J, Kučera T. Bioptic study of left and right atrial interstitium in cardiac patients with and without atrial fibrillation: interatrial but not rhythm-based differences. *PLoS One.* 2015;10:e0129124. doi: 10.1371/journal.pone.0129124

27. Li B, Luo F, Luo X, Li B, Qi L, Zhang D, Tang Y. Effects of atrial fibrosis induced by mitral regurgitation on atrial electrophysiology and susceptibility to atrial fibrillation in pigs. *Cardiovasc Pathol.* 2019;40:32–40. doi: 10.1016/j.carpath.2019.01.006

28. Caixal G, Althoff T, Garre P, Alarcón F, NuñezGarcia M, Benito EM, Borras R, Perea RJ, Prat-González S, Gunturiz C, et al. Proximity to the descending aorta predicts regional fibrosis in the adjacent left atrial wall: aetiopathogenic and prognostic implications. *Europace.* 2021;23:1559–1567. doi: 10.1093/europace/euab107

29. Akoum N, McGann C, Vergara G, Badger T, Ranjan R, Mahnkopf C, Kholmovski E, Macleod R, Marrouche N. Atrial fibrosis quantified using late gadolinium enhancement MRI is associated with sinus node dysfunction requiring pacemaker implant. *J Cardiovasc Electrophysiol.* 2012;23:44–50. doi: 10.1111/j.1540-8167.2011.02140.x

30. Hiram R, Xiong F, Naud P, Xiao J, Sirois M, Tanguay J-F, Tardif J-C, Nattel S. The inflammation-resolution promoting molecule resolvin-D1 prevents atrial proarrhythmic remodelling in experimental right heart disease. *Cardiovasc Res.* 2021;117:1776–1789. doi: 10.1093/cvr/cvaa186

31. Mrgulescu AD, Nuñez-Garcia M, Alarcón F, Benito EM, Enomoto N, Cozzari J, Chipa F, Fernandez H, Borras R, Guasch E, et al. Reproducibility and accuracy of late gadolinium enhancement cardiac magnetic resonance measurements for the detection of left atrial fibrosis in patients undergoing atrial fibrillation ablation procedures. *Europace.* 2019;21:724–731. doi: 10.1093/europace/euy314

32. Igawa O, Adachi M, Yano A, Miake J, Inoue Y, Ogura K, Kato M, Tanaka H, Iitsuka K, Hisatome I, et al. Extension of the inferior vena cava into the posteroinferior right atrium. *Heart Rhythm.* 2006;3:1481–1485. doi: 10.1016/j.hrthm.2006.08.031

SUPPLEMENTAL MATERIAL

Data S1. Supplemental Methods

LGE-CMR imaging

Acquisition protocol: Images were obtained with a 3.0 Tesla CMR (Magnetom Prisma Siemens Healthcare, Germany) and a dedicated 32-channel cardiac coil. LGE-CMR scans were acquired 20 min after an intravenous bolus injection of 0.2 mmol/kg gadobutrol (Gadovist, Bayer Hispania) using a free-breathing 3D navigator and ECG-gated inversion-recovery gradient-eco sequence applied in the axial orientation. The voxel size was 1.25x1.25x2.5 mm. Repetition time/echo time was 2.3/1.4 ms; flip angle, 11º; bandwidth, 460 Hz/pixel; inversion time (TI) 280 to 380 ms; and parallel imaging with GRAPPA technique, with reference lines of R=2 and 72. A TI scout sequence was used to nullify the left ventricular myocardial signal and determine optimal TI. Typical scan time for LGE-CMR sequence was 15 minutes (11-18), depending on heart rate and breathing patterns.

Post-processing: RA and LA segmentation was performed using ADAS 3D software (Barcelona, Spain). Atrial contours of the wall were manually drawn by two expert operators in each axial plane of the LGE-CMR, without invading the interatrial common septum, and a tridimensional model was constructed. ADAS automatically builds a 3D shell. Subsequently, pulmonary veins at the ostium level, mitral valve plane and left appendage were excluded in the LA, and the superior and inferior vena cava at the ostium level, tricuspid valve plane and coronary sinus were excluded in the RA.

Signal intensity was internally (within each patient) normalized to blood pool intensity to provide an absolute signal intensity value that would allow comparisons between patients. The LA blood pool was automatically identified by the software. It was chosen both for LA and RA wall normalization because it was found to be less

variable than the RA blood pool. Image Intensity Ratio (IIR) was calculated as the ratio between the signal intensity of each single pixel and the mean blood pool intensity for each patient. Each IIR value was colour-coded as healthy (IIR<1.20), interstitial fibrosis (1.20≤IIR≤1.32) and dense scar (IIR≥1.32) using previously standardized thresholds for the LA.[11] Dense scar threshold was defined as those fibrotic patches that were predicted conduction block in re-do procedures. Interstitial fibrosis was defined as atrial tissue with IIR lying between the normality-fibrosis boundary (average IIR + 2SDs in a healthy volunteer cohort) and the dense scar threshold.[11] Of note, however, formal histological validation is missing.

Sphericity assessment: Sphericity evaluates the variation between the chamber and the sphere that best fitted its shape. The radius of such sphere is calculated as the mean of distances between all points of the atrium wall and the center of mass (average radius-AR). Finally, the coefficient of variation of the sphere (CVS = AR standard deviation/AR) was obtained to define the atrium sphericity [(1- CVS)*100]. A comprehensive technical description of the method is provided in its original description[13] and its Supplemental Methods (https://onlinelibrary.wiley.com/action/downloadSupplement?doi=10.1111%2Fjce.121 16&file=jce12116-sup-0001-S1.doc). The final sphericity number is a unitless value which may potentially be from 0 to 100 (a perfect sphere), but common values in the LA range from 70 to 90.[13] No previous data are available for the RA.

Table S1. Correlation between RA and LA remodeling parameters for total population and by subgroups.

RA / LA correlation	Overall		Healthy volunteers		Paroxysmal AF		Persistent AF	
	R Pearson	P	R Pearson	P	R Pearson	P	R Pearson	P
Volume (mL)	0.695	<0.0001	0.457	0.25	0.426	0.001	0.581	<0.0001
Surface (cm²)	0.725	<0.0001	0.473	0.2	0.600	<0.0001	0.547	<0.0001
Total fibrosis (%)	0.589	<0.0001	0.837	0.005	0.468	<0.0001	0.679	<0.0001
Interstitial fibrosis (%)	0.463	<0.0001	0.713	0.031	0.460	<0.0001	0.450	0.002
Dense scar (%)	0.638	<0.0001	0.67	0.054	0.406	0.002	0.784	<0.0001
Sphericity	-0.010	0.92	0.12	0.75	-0.050	0.72	-0.222	0.14

*Abbreviations: AF: atrial fibrillation; LA: left atrium; RA: right atrium

Table S2. Prediction models of RA remodeling - total fibrosis (%), area (cm2) and sphericity- between clinical, electrocardiographic, and echocardiographic parameters, using univariate and multivariate linear regression analysis.

	Univariate			Multivariate		
	Beta	**95% CI**	**p**	**Beta**	**95% CI**	**p**
RA FIBROSIS (%)						
Age	0.05	-0.08 to 0.18	0.45			
Female sex	-0.34	-3.36 to 2.67	0.82			
Bundle branch block	**4.13**	**-0.19 to 8.44**	**0.006**			
QRS	-0.04	-0.10 to 0.03	0.293			
PR	-0.03	-0.08 to 0.01	0.12			
BMI	0.19	-0.05 to 0.42	0.12			
Hypertension	-0.05	-2.81 to 2.70	0.97			
Diabetes	**7.71**	**2.92 to 12.5**	**0.002**	**7.70**	**2.81 to 12.5**	**0.002**
Sleep apnea	1.83	-2.53 to 6.18	0.41			
Atrial Flutter	0.35	-4.02 to 4.72	0.87			
AF pattern	0.08	-2.68 to 2.84	0.96			
LVEF	0.04	-0.15 to 0.22	0.71			
LA diameter	0.16	-0.08 to 0.40	0.19			
TR ≥ moderate	3.52	-0.65 to 7.68	0.10			
RA AREA (cm^2)						
Age	0.01	-0.48 to 0.52	0.96			
Female sex	**-12.57**	**-23.7 to -1.4**	**0.028**	**-14.95**	**-24.9 to -4.94**	**0.004**
Bundle branch block	5.10	-11.6 to -21.8	0.545			
QRS (ms)	-0.01	-0.27 to 0.25	0.92			
PR (ms)	**0.13**	**-0.03 to 0.29**	**0.11**	**0.15**	**0.011 to 0.28**	**0.034**
BMI	0.43	-0.46 to 1.32	0.34			
Hypertension	-3.32	-13.83 to 7.19	0.53			
Diabetes	-3.25	-21.6 to 15.1	0.73			
Sleep apnea	8.57	-8.12 to 25.25	0.31			
Atrial flutter	-3.61	-20.4 to 13.2	0.67			
AF pattern	**27.77**	**18.8 to 36.7**	**<0.0001**	**26.3**	**17.4 to 35.2**	**<0.0001**
LVEF	**-0.801**	**-1.49 to 0.11**	**0.02**			
LA diameter	**1.37**	**0.49 to 2.26**	**0.003**			
TR ≥ moderate	**13.17**	**-2.82 to 29.2**	**0.11**	**12.9**	**-1.11 to 26.9**	**0.07**
RA SPHERICITY						
Age	-0.021	-0.07 to 0.03	0.41			

|						
Female sex	0.534	-0.63 to 1.70	0.36			
Bundle branch block	0.163	-1.53 to 1.86	0.85			
QRS (ms)	-0.003	-0.03 to 0.02	0.85			
PR (ms)	<0.001	-0.02 to 0.02	0.96			
BMI	0.026	-0.07 to 0.12	0.57			
Hypertension	-0.50	-1.56 to 0.57	0.36			
Diabetes	-1.30	-3.15 to 0.55	0.17			
Sleep apnea	-0.14	-1.85 to 1.57	0.87			
Atrial Flutter	0.10	-1.61 to 1.81	0.91			
AF pattern	0.85	-0.21 to 1.92	0.11			
LVEF	-0.05	-0.12 to 0.02	0.17			
LA diameter	-0.03	-0.12 to 0.07	0.59			
TR ≥ moderate	**1.55**	**-0.06 to 3.17**	**0.06**	**1.47**	**-0.17 to 3.10**	**0.08**

*Abbreviations: AF: atrial fibrillation; BMI: body mass index; LA: left atrium; LVEF: left

ventricular ejection fraction; RA: right atrium; TR: tricuspid regurgitation

**Figure S1. Correlation between RA remodeling parameters.**
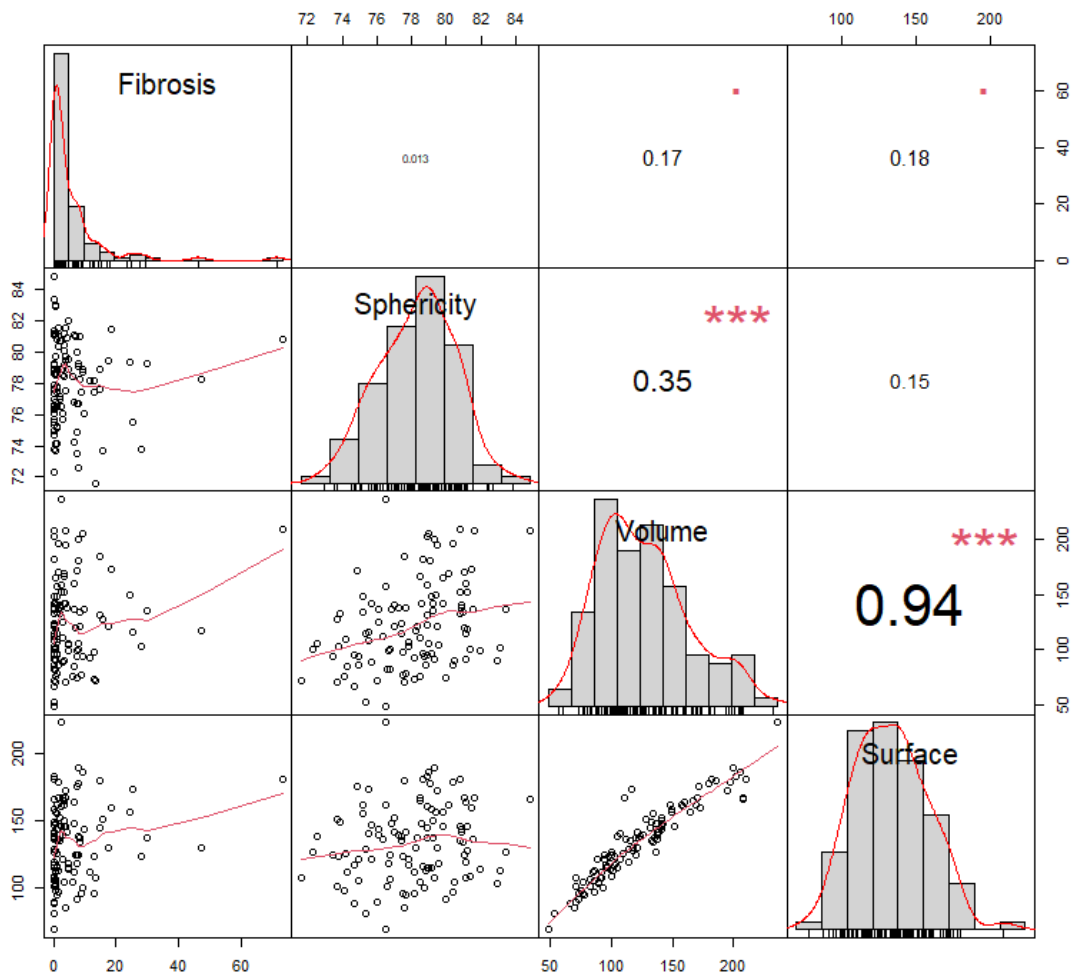
The diagonal cells show the distribution of each fibrosis, sphericity, volume, and surface.

In the lower-left corner, their bivariate scatter plot is shown in the intersection cell. In

the upper-right corner, the magnitude of their correlation (Pearson coefficient) is shown

in number, and the significance in asterisks (***p<0.001; • 0.10<p<0.05; no sign means

p>0.1).

Figure S2. Bar chart representing percentage of AF patients with fibrosis in RA and LA (total fibrosis and breakdown by type of fibrosis).
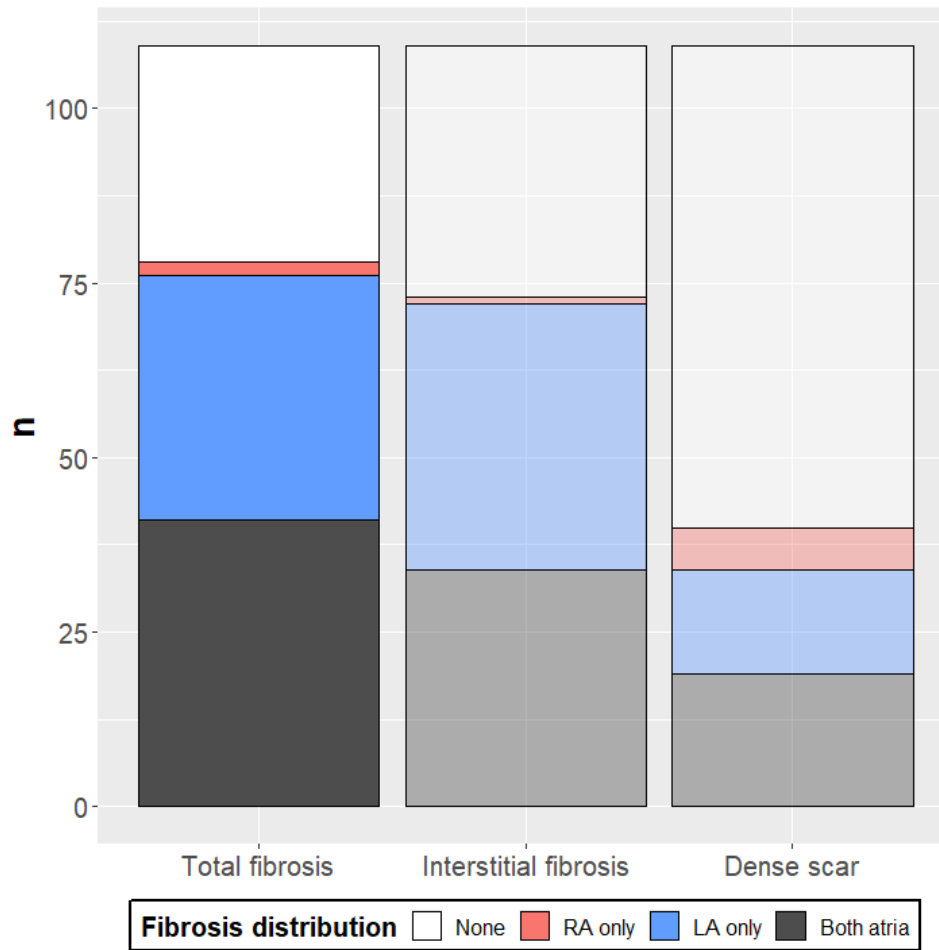

*LA: left atrium; RA: right atrium

Figure S3. Pairwise comparisons of atrial fibrosis burden for each of the RA regions.
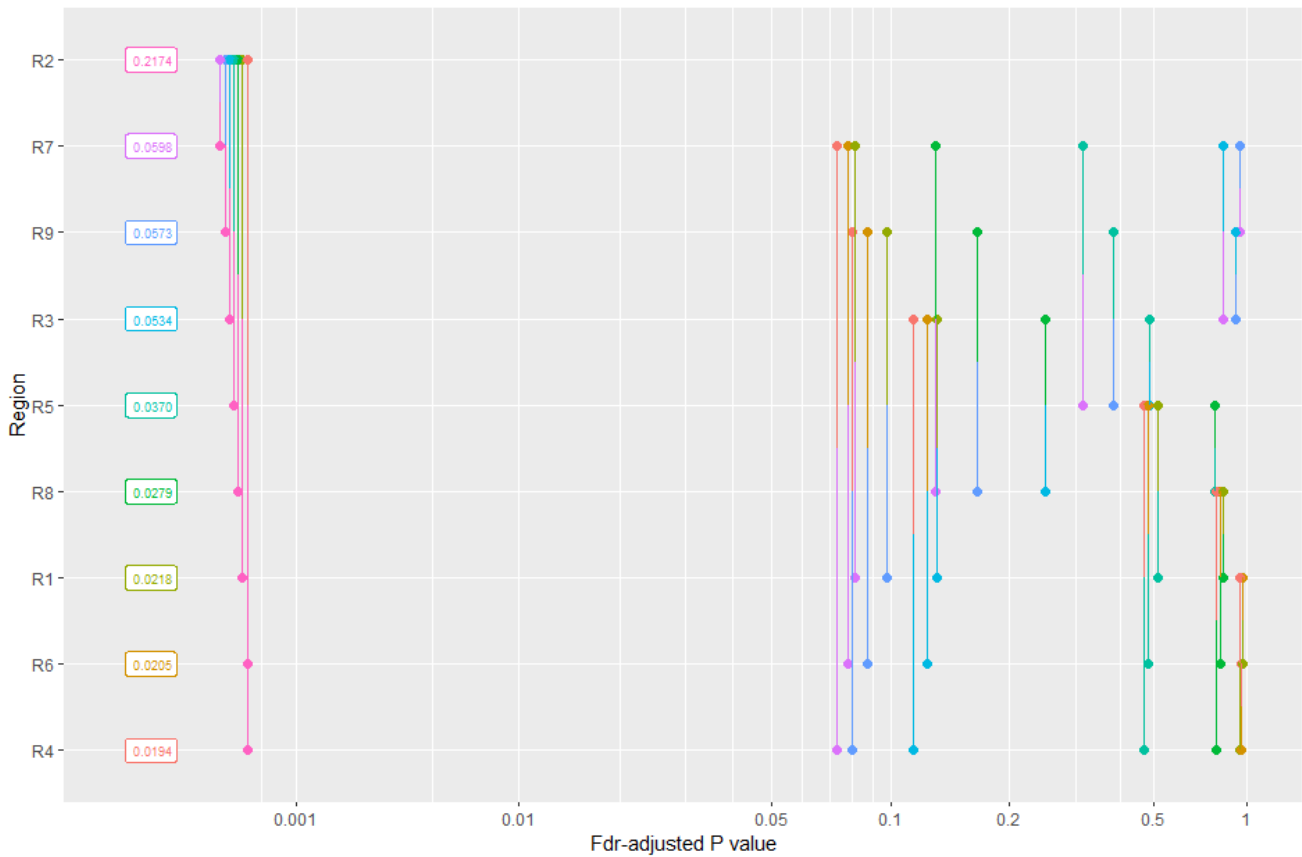
Each region is plotted in the Y-axis (top to low: higher to lower fibrosis burden, labels).

Segments linking two regions are plotted in the X-axis value corresponding to the fdr-adjusted p-value of their pairwise comparison.

Figure S4. Anatomical relationship between right and left atria and ascending and descending aorta.
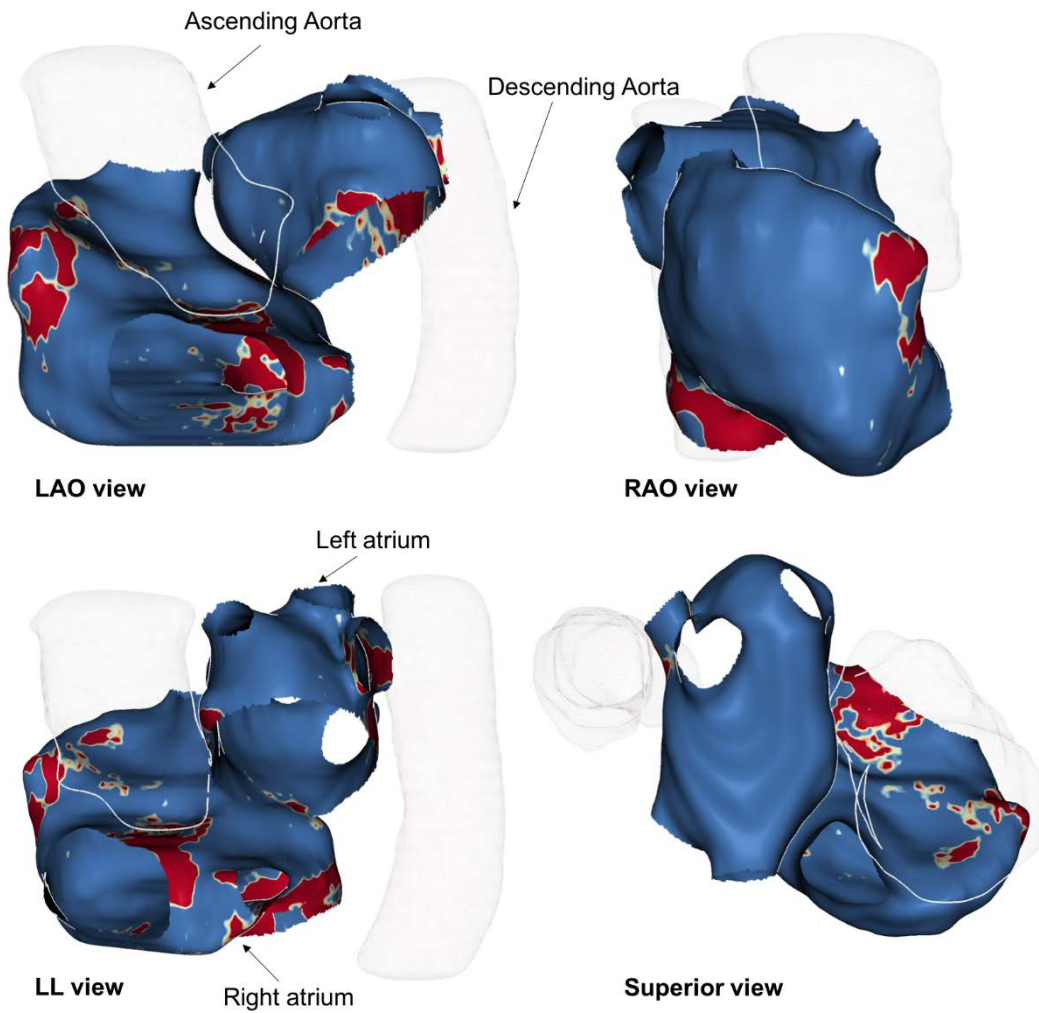
3D shells postprocessed together.

*LAO: left anterior oblique; LL: left lateral; RAO: right anterior oblique